Journal of Power Sources 225 (2013) 129–136

Contents lists available at SciVerse ScienceDirect

Journal of Power Sources

journal homepage: www.elsevier.com/locate/jpowsour

Synthesis of self-supported non-precious metal catalysts for oxygen reduction reaction with preserved nanostructures from the polyaniline nanofiber precursor

Yang Hu [a,b], Xiao Zhao [a,b], Yunjie Huang [c], Qingfeng Li [c], Niels J. Bjerrum [c], Changpeng Liu [d,*], Wei Xing [a,*]

[a] State Key Laboratory of Electroanalytical Chemistry, Changchun Institute of Applied Chemistry, Chinese Academy of Sciences, Changchun 130022, China
[b] Graduate School of the Chinese Academy of Sciences, Beijing 100039, China
[c] Department of Energy Conversion and Storage, Technical University of Denmark, Kemitorvet 207, DK-2800 Kgs. Lyngby, Denmark
[d] Laboratory of Advanced Power Sources, Changchun Institute of Applied Chemistry, Chinese Academy of Sciences, Changchun 130022, China

HIGHLIGHTS

- Novel preparation of self-supported and nano-structured NPMCs for ORR.
- An onset potential of 0.905 V *vs.* RHE and nearly four-electron ORR pathway.
- Effects of ferrous species in precursors on the final catalysts explored.
- Onset ORR potentials increasing with the initial Fe content from 0 to 3.0 wt.%.

ARTICLE INFO

Article history:
Received 3 August 2012
Received in revised form
5 October 2012
Accepted 8 October 2012
Available online 15 October 2012

Keywords:
Oxygen reduction reaction
Non-precious metal catalyst
Heat-treatment
Activity
Active site

ABSTRACT

Non-precious metal catalysts (NPMCs) for the oxygen reduction reaction (ORR) are an active subject of recent research on proton exchange membrane fuel cells. In this study, we report a new approach to preparation of self-supported and nano-structured NPMCs using pre-prepared polyaniline (PANI) nanofibers as both nitrogen and carbon precursors. The synthesized NPMCs possess nanoworm structures preserved from the PANI precursor and exhibit high onset potential of 0.905 V *vs.* RHE and selective activity of nearly four-electron ORR pathways. A significant enhancement in the intrinsic activity and onset potential for the ORR is observed when the Fe content in the precursor is increased from 0 to 3.0 wt.%, while further addition to 10.0 wt.% results in a decrease in the catalytic activity.

1. Introduction

Insufficiently active catalysts for the oxygen reduction reaction (ORR) have long been regarded as the major impediment to the commercialization of polymer exchange membrane fuel cells (PEMFCs) [1,2]. The state-of-the-art cathode catalysts for PEMFCs are based on platinum and its alloy nanoparticles, which are suffering from the prohibitive cost and limited resources. Great efforts have been devoted to reduction or substitution of the precious metals in the catalysts. The development of non-precious metal catalysts (NPMCs) is one of the most active subjects of this area [3–5].

A few types of NPMCs are under extensive development for PEMFC applications, including non-pyrolyzed transition metal nitrogen-containing complexes [6], carbon-supported transition metal/nitrogen materials [7], metal oxide/carbide/nitride materials [8], enzymatic compounds [9], and others. Among these NPMCs, the carbon-supported transition metal/nitrogen (M–N_x/C, M = Co, Fe, Ni, *etc.*) materials are of particular interest. The M–N_x/C based catalysts have been under development for decades since the work by Jasinski [10] and Yeager [11]. Significant improvement of both the catalytic activity and stability has been achieved by a pyrolytic treatment of the transition metal-containing macrocycle compounds at typical temperatures of 500–1000 °C in an inert gas atmosphere. It was believed from the earlier years that the macrocycle compounds as the precursor were essential for the catalytic activities towards ORR. This understanding was, however, not completely true, as Gupta et al. [11] demonstrated that active NPMCs could also be prepared by pyrolyzing polyacrylonitrile

* Corresponding authors. Tel.: +86 431 85262223; fax: +86 431 85685653.
E-mail addresses: liuchp@ciac.jl.cn (C. Liu), xingwei@ciac.jl.cn (W. Xing).

0378-7753/$ – see front matter
http://dx.doi.org/10.1016/j.jpowsour.2012.10.013

(PAN), iron salt and VulcanXC-72 carbon black under Ar. Since then, a variety of combinations of simple metal, nitrogen and carbon precursor materials have been investigated to replace the often-expensive macrocycles [12].

The nitrogen precursors can be many kinds of nitrogen containing chemicals or even NH_3. As an example, nitrogen containing conducting polymer proves a good nitrogen precursor to create catalytically active sites of the M–N_x/C catalysts [13,14]. The characteristic feature of thus prepared NPMCs under an inert atmosphere of Ar or N_2 during the heat-treatment, in general, results in more stable catalysts. For example, Bashyam and Zelenay [6] synthesized NPMCs with polypyrrole (PPy) as the nitrogen source with improved performance durability, while Wu et al. [7,13,15,16] pyrolyzed polyaniline(PANI)/C–Fe(Co) complex and obtained catalysts with an enhanced activity and performance stability. When NH_3 was used as the nitrogen precursor, the activity of prepared catalyst was generally higher though the stability would be decreased [17]. Lefevre et al. [2] synthesized very active NPMCs utilizing NH_3 as the nitrogen precursor, however with a fast performance degradation. Other nitrogen sources including graphitic C_3N_4 [18], polyacrylonitrile (PAN) [19] and ethylenediamine (EDA) [20] have also been employed to prepare NPMCs.

In terms of carbon precursors, high specific surface area carbon supports (carbon blacks or nanotubes) were typically used to support and facilitate the formation of the catalytically active sites [21] when NH_3 and metal-containing inorganic salts were employed as nitrogen and metal precursors, respectively [2,22]. Not only were the carbon supports functioning as carbon precursors but also facilitating to achieve a porous structure of the NPMCs. In cases where nitrogen/carbon-containing polymers were used as nitrogen precursors [16], the incorporation of carbon supports was primarily for the purpose of optimizing the porous structure of final catalyst. As recently reported the carbon phase derived from these polymers themselves was capable of hosting a significant number of active sites [7]. In other words, a supplementary carbon source might have diluted the active sites, which in turn would have resulted in the low active site density of the Fe_xN-based catalysts. From synthetic points of view, NPMCs prepared without using additional carbon supports, i.e. the self-supported NPMCs, might have a higher active site density and better catalytic activity as long as the morphologies and porous structures of the carbon phases derived from the carbon–nitrogen-containing precursors could be somehow tailored.

Following this consideration, we have noticed that the nanostructures of some PANIs could be preserved after the heat-treatment under certain conditions, as reported by Zhu et al. [23] and other researchers [24,25]. Stimulated by this idea along with the fact that PANI as a conducting polymer has been extensively studied as a nitrogen precursor for preparation of NPMCs with high ORR activity, we proposed here a new approach to preparation of the self-supported Fe_xN-based NPMCs by employing nano-structured PANI as both the nitrogen and carbon precursors aiming at preservation of the nanostructures of the precursors. Although some indirect methods have been reported such as the use of foaming agents (FeC_2O_4) [26] or silica hard template [27], to the best of our knowledge, this is the first time to explore the synthesis of self-supported NPMCs with tailored nanostructures by means of controlling the morphologies and structures of the precursors.

Besides, there was another important motivation for the present work. It is well known that the promotional effect of transition metals in the precursor on the ORR activity is not unambiguously understood. Dodelet et al. [2,28] claimed that the ORR active sites involved the metal species, while other researchers [29,30] suggested that the transition metal species just played a role in the formation of active sites either by catalyzing the doping of nitrogen atoms into carbon or electronically changing the reactive environment. As the molecular structures of the precursors were destroyed during the heat-treatment, leading to highly heterogeneous products, it was not straightforward to conclude the effect. Herein we tried to find some clues to clarify this issue in association of the synthesis of the self-supported NPMCs. First of all, the PANI as the nitrogen and carbon precursor was ex-situ polymerized. The un-reacted monomers and other reactants or byproducts, which otherwise would be present during the following synthesis of the NPMCs, were removed, i.e. the synthesized PANI was collected, purified and used for the catalyst synthesis. By doing so, the constituents of the catalyst precursor were well defined and the initial metal content in the precursor could be precisely controlled in this work. Besides, no additional carbon supports were added and therefore the possible contamination of metallic impurities from the carbon blacks was avoided.

2. Experimental

2.1. Synthesis of polyaniline (PANI)

PANI nanofibers were synthesized according to a procedure described previously with minor modifications [31]. Aniline was distilled twice before use. All other chemicals were of analytical grade and used without further purification. Typically, 1.9 ml of freshly distilled aniline was dissolved in 100 ml of the 1 M doping acid while 5.7 g of ammonium peroxydisulfate (APS) was dissolved separately in 100 ml of the 1 M doping acid. Then, the APS solution was added quickly to the above aniline mixture solution. It gave an aniline to APS molar ratio of 1:1.25. Two types of doping acids, *p*-Toluenesulfonic Acid (PTSA) and HCl, were attempted and the resultant polymers were hereafter referred to as PANI-1 and PANI-2, respectively. After that, a 2 ml of aqueous sodium hypochlorite (5 wt.%) solution was added under agitation. At last, the reaction vessel was left without stirring for 25 min. To illustrate the effect of APS on the PANI synthesis, another batch of PANI was prepared with HCl as the doping acid while the molar ratio of aniline to APS was kept to be 4:1 (by adding 1.14 g APS instead of 5.7 g). Thus synthesized polymer was referred to as PANI-3. The precipitated PANI polymer was filtered, washed sequentially with the doping acid, deionized (DI) water, and acetone, finally followed by drying at 80 °C overnight. The average diameter for different sample was obtained by measuring the sizes of about 100 randomly chosen particles in several magnified SEM images for each sample, while the average length was determined by measuring sizes of about 50 particles with well-defined dimensions.

2.2. Catalyst preparation

The precursor suspension was prepared by adding a certain amount of $FeCl_3$ into a dispersion of the PANI (400 mg) in 200 ml DI water. The mass content of Fe as expressed as Fe/(Fe + PANI) was 0, 0.3, 0.5, 1.0, 3.0, 5.0 and 10.0 wt.%, respectively. The resulting suspension was stirred and ultrasonically blended for 12 h, followed by drying at 80 °C for 24 h. Finally, the precursor powder was grounded and transferred to a quartz boat and heat-treated at 900 °C for 1 h under a flow rate of 100 ml min^{-1} of N_2 in a horizontal quartz tube furnace. Before starting the heat-treatment, the horizontal quartz tube was evacuated and purged with nitrogen twice to remove traces of oxygen. The furnace used was slidable which could achieve fast heating and cooling with well defined durations of the heat-treatment. The furnace was heated at the temperature ramping rate of 15 °C min^{-1} and cooled under N_2 from 900 °C to 60 °C in *ca.* 3 min. After cooling, the catalyst was ground again and leached in 0.5 M H_2SO_4 at 80 °C for 8 h to remove any dissolvable species, followed by washing with DI water and drying at 80 °C under vacuum. The finally

obtained catalyst was denoted as *X*Fe–PANI-L. In a few occasions the obtained catalysts were not subject to the acid leaching process and hereafter referred to as *X*Fe–PANI. In these abbreviations *X* is the initial Fe mass content in the precursor.

2.3. Electrochemical measurement

Electrochemical measurements were conducted using PARSTAT 273 advanced electrochemical system. A catalyst ink was prepared by dispersing 10 mg of the catalyst powder ultrasonically in a mixture solution containing 95 μL Nafion (5 wt.%) solution and 570 μL ethanol. The catalyst film coated electrode was obtained by dispersing the catalyst ink on a glassy carbon rotating disk electrode (RDE) followed by drying in air. The catalyst loading of 0.6 mg cm^{-2} for NPMC was used in this work. A conventional three-electrode cell was employed incorporating a saturated calomel electrode (SCE) as the reference electrode, a Pt foil as the counter electrode and the catalyst film coated RDE as the working electrode. The electrolyte was an H_2SO_4 solution of pH 1 for NPMCs and an $HClO_4$ solution of pH 1 for Pt/C [32]. RDE measurements were conducted by liner sweep voltammetry (LSV) at different rotating speeds from 250 to 2500 rpm. The LSV was carried out in the H_2SO_4 solution first saturated with O_2 and then with N_2. The ORR current (i_{ORR}) was determined by subtracting the current measured in the N_2 saturated solution from that in the O_2 saturated solution. The onset ORR potentials were defined as the electrode potential at the $i_{ORR} = 3$ μA cm^{-2}. For comparison, the ORR data of the commercial Pt/C catalyst (20 wt.%, E-TEK) with a loading of 40 μg_{Pt} cm^{-2} were also recorded. All experiments were carried out at 25 °C in a thermostatic bath. In all figures, the potentials were converted to values versus the reversible hydrogen electrode (RHE). EIS measurements were performed under open circuit potential between 100 kHz and 0.1 Hz with an excitation signal of 5 mV. To analyse their impedance parameters, the impedance spectra were fitted by the Zsimpwin program.

2.4. Physical characterizations

X-ray photoelectron spectroscopy (XPS) measurements were carried out on a Kratos XSAM-800 spectrometer with an Mg Kα radiation source. The binding energy was calibrated by placing the principal C 1s peak at 284.6 eV. X-ray diffraction (XRD) measurements were performed with a PW1700 diffractometer (Philips Co.) using a Cu K_α ($\lambda = 1.5405$ Å) radiation source. Transmission electron microscope (TEM) images were obtained with Philips TECNAI G2 at 200 kV. SEM (scanning electron microscope), Energy-dispersive X-ray spectroscopy (EDX) and electron backscatter diffraction (EBSD) images were taken on LEO 1525 FE-SEM scanning electron microscope.

3. Results and discussion

3.1. Catalyst morphologies

Fig. 1 shows the typical SEM images of obtained PANI-1, PANI-2, PANI-3 nanofibers and their corresponding final NPMCs with an initial Fe content of 1.0 wt.%. PANI-1 and PANI-2, as prepared with PTSA and HCl as the doping acid, respectively, and the molar ratio of aniline to APS of 1:1.25, had similar diameters (*ca.* 170 nm) but different lengths of about 2 μm for PANI-1 and about 1 μm for PANI-2. As to PANI-3, which was prepared with HCl as the doping acid but with a high aniline to APS molar ratio of 4:1, the polymer was also in a nanofiber shape with a similar length of about 1 μm but a much smaller diameter (*ca.* 90 nm). It seems that the doping acid would affect the length of prepared PANI nanofibers while the molar ratio of aniline to APS would affect the diameter of them.

For catalysts prepared from these three kinds of polymers, the nanofiber shapes of the used PANI precursors were well preserved, though with shrinkages to some extent, leading to nanowarm-like particles. Catalysts prepared from PANI-1 and PANI-2 possessed similar diameters of *ca.* 100–120 nm while the PANI-3-based catalyst presented a correspondingly smaller diameter (*ca.* 70 nm). In cases of other catalysts prepared with different initial contents of Fe, similar phenomena were observed (not shown here). Recently Wu et al. [7,16] reported that, when the PANI was in-situ polymerized and deposited onto carbon black supports, the initial morphology of PANI, which was similar to that in the present study, gradually disappeared and spherical particles were formed as the heat-treatment temperature was increased to 600 °C. In the

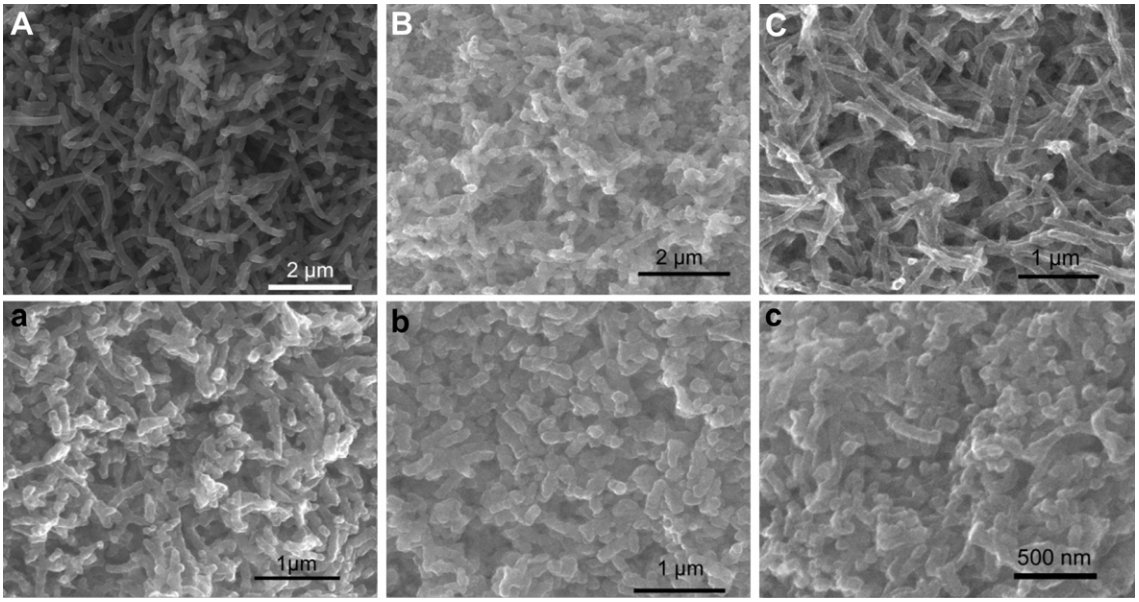

Fig. 1. SEM images of PANI nanofibers: (A) PANI-1, (B) PANI-2, (C) PANI-3 and the corresponding final catalysts with initial Fe content of 1.0 wt.%: (a) 1.0Fe–PANI-1-L, (b) 1.0Fe–PANI-2-L, (c) 1.0Fe–PANI-3 L.

present study, without carbon supports in the precursors, the obtained catalysts preserved the initial morphology of PANI precursors, which suggested the significance of the carbon supports during the carbonization process of PANI. Carbon supports might be involved in the process of the polymer condensation during the heat-treatment, which led to deposition of the CN_X composites on their surface in irregular shapes. In the absence of carbon supports as in the present work, the carbonization of PANI/Fe complex alone would lead to the formation of CN_X composites with the preserved morphology of the initial PANI precursors. The evolution mechanism of the PANI nanofiber morphology during the pyrolysis is not clear thus far, however, Trchová et al. [33] have proposed that the cross-linking reaction and nitrogen atoms in the polymer played important roles in stabilization of supramolecular structure during the pyrolysis.

This interesting phenomenon provides an approach to preparation of the self-supported NPMCs by employing nano-structured precursors. It is well known that PANI and PPy can be synthesized with a variety of nanostructures *e.g.*, in forms of nanoparticles, nanofibers, nanotubes, and nano/microspheres, *etc.* [34–37]. In this way, a large variety of self-supported NPMCs with tailored nanostructures and desired specific surface area, pore sizes could be prepared. Further exploration of this approach, such as employing PANI nanospheres and nanotubes in the synthesis, is under way. In the following sections, however, the electrochemical and physical characterizations were made based on catalysts prepared from the PANI-2 polymer.

3.2. Electrochemical characterizations

Electrochemical evaluation was made for a series of *X*Fe–PANI-L catalysts with different initial Fe contents. Fig. 2 shows the ORR polarization curves in the low over-potential region for the prepared catalysts as well as the commercial Pt/C catalyst. Fig. 3 presents the RDE current–potential curves for the best catalyst (3.0Fe–PANI-L) among this series of catalysts at various rotating rates. The onset potential of 3.0Fe–PANI-L for the ORR was found to at 0.905 V *vs.* RHE, which was about 0.1 V lower than that of the commercial Pt/C catalyst (1.05 V *vs.* RHE). This value was close to that of the best PANI-based catalysts reported in literature [16]. The ORR activities were further investigated using the Koutecky–Levich equations [38]:

$$\frac{1}{J} = \frac{1}{J_L} + \frac{1}{J_K} = \frac{1}{B\omega^{1/2}} + \frac{1}{J_k} \quad (1)$$

$$B = 0.62nFC_0(D_0)^{2/3}\nu^{-\frac{1}{6}} \quad (2)$$

where J is the measured current density, J_K is the kinetic current density, J_L is the diffusion-limited current density, ω is the electrode rotation rate, F is the Faraday constant (96485 C mol^{-1}), C_0 is the bulk concentration of O_2 (1.3×10^{-3} mol L^{-1}), D_0 is the diffusion coefficient of O_2 (1.9×10^{-5} cm^2 s^{-1}) and ν is the kinetic viscosity of the electrolyte (1.0×10^{-2} cm^2 s^{-1}) [22]. The inset of Fig. 3 shows the Koutecky–Levich plots for the ORR on 3.0Fe–PANI-L. The slopes remain approximately constant over the potential range from 0.1 to 0.5 V, which suggests that the electron transfer numbers for the ORR at different potentials are similar. In cases of other catalysts, similar phenomena were observed (not shown here). The electron transfer number (n) for 3Fe–PANI-L derived from the slope was *ca.* 3.99, which was similar to that of the commercial Pt catalyst (*ca.* 3.95). Similarly Wu et al. [13] reported a nearly four-electron ORR pathway for the best PANI-based catalysts. In summary, the high onset potential and near four-electron transfer number of 3.0Fe–PANI-L reflected the high intrinsic activity and selectivity of the prepared catalyst, which testified that this approach could preserve the active site structures as those catalysts prepared employing the in-situ polymerized PANI and carbon supports. It should be noted here, however, that all the six catalysts exhibited low limiting current densities and half-wave potentials as compared with the literature [7], apparently due to the poor mass transportation on the catalysts. This was not surprising as the catalysts were in a worm-like shape with a diameter of about 100 nm. It is anticipated that NPMCs with better mass transport behaviours might be obtained by employing PANI nanotubes, nanospheres, or other 3-D nanostructures as the precursor. It is interesting to notice that a kind of urchin-like hollow PANI spheres have been recently reported to be able to maintain their morphology after a heat-treatment at 1200 °C [23].

Efforts were made to investigate the promotional effects of the ferrous species on the ORR activity for the prepared catalysts from different initial Fe contents in the precursors. The mass specific

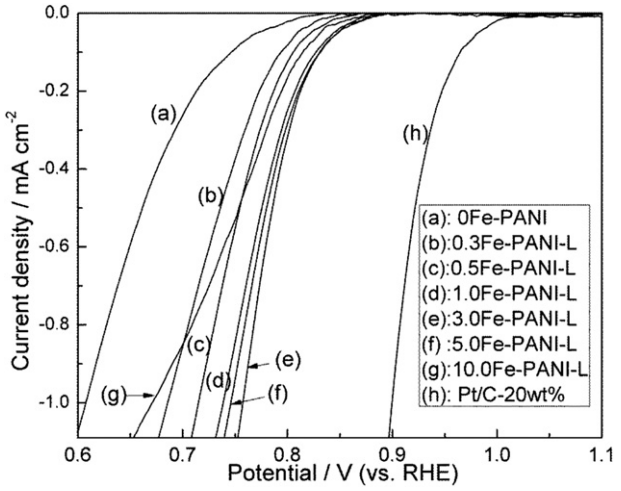

Fig. 2. ORR polarization curves for different catalysts in the low over-potential region: (a) 0Fe–PANI, (b) 0.3Fe–PANI-L, (c) 0.5Fe–PANI-L, (d) 1.0Fe–PANI-L, (e) 3.0Fe-PANI-L, (f) 5.0Fe–PANI-L (g) 10.0Fe–PANI-L and (h) Pt/C in O_2 saturated solution of pH 1 at 1000 rpm. Scan rate: 10 mV s^{-1}. Electrolyte: H_2SO_4 for NPMCs and $HClO_4$ for Pt/C. Catalyst loading: 0.6 mg cm^{-2} for NPMCs and 40 μg_{Pt} cm^{-2} for Pt/C.

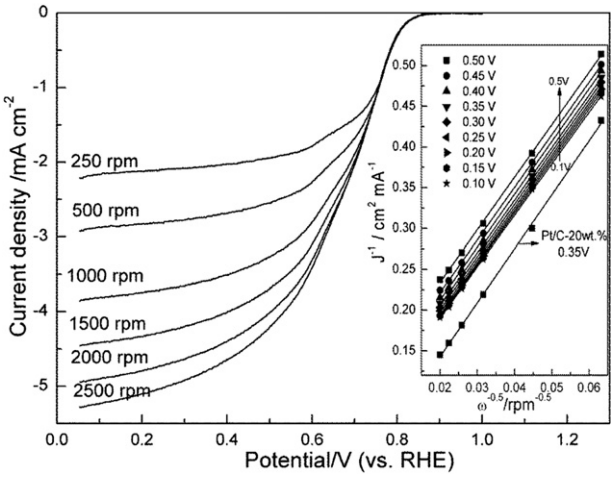

Fig. 3. ORR polarization curves for 3.0Fe–PANI-L at different rotation rates. The inset shows the Koutecky–Levich plots of 3.0Fe–PANI-L at a potential range of 0.1–0.5 V and the commercial Pt/C catalyst at 0.35 V.

activities at 0.8 V (J_k) derived from Tafel plots (not shown here) and the onset ORR potentials for the series of catalysts are compared, as shown in Fig. 4. It is clear from this figure that as the initial Fe content was increased from 0 to 3.0 wt.%, the J_k was steadily increasing. Further addition of the metal to 10.0 wt.%, however, resulted in a decrease in the catalytic activity. Besides, it is of special interest to note that the 0Fe–PANI catalyst, as prepared without any transition metal added in the synthesis process, showed a noticeable catalytic activity towards ORR. Further addition of the Fe species in the precursor dramatically improved the activity of the catalyst towards ORR. Similar trend was observed for the onset ORR potential, the variation of which is believed to be attributable to the nature, rather than the number, of the catalytically active sites.

Fig. 5 presents the cyclic voltammograms (CVs) recorded in N_2 saturated H_2SO_4 solution at a scan rate of 10 mV s^{-1}. The potential window between 0.4 and 0.8 V is an indicator of capacitive current depending on the electrochemically accessible area [39]. A pair of well-identified redox peaks at *ca.* 0.64 V and 0.61 V were observed, the height of which had an obvious dependence on the initial Fe content, especially from 0 to 1.0 wt.%. Considering the high oxygen surface content of these catalysts (especially 0Fe–PANI as to be seen from the XPS results below), the pair of peaks did not seem to be mainly derived from quinone–hydroquinone groups on the catalyst surface. As pointed out in literature, this pair of peaks could be originated from surface confined iron oxide (FeO_x) particles in the final catalyst [40,41]. Considering the similar elemental composition of the samples and that these peaks were not observed in the present work for the catalysts prepared with no or low contents of Fe in the precursors, it was speculated that the origin of them was most likely from the surface confined FeO_x species in the final catalysts. No defined FeO_x characteristic peaks in the XRD analysis (as seen below) were, however, observed, likely due to the very low concentration and/or poor crystallinity of the FeO_x species. Anyhow, these metal oxide species possessed little ORR activity [40] and are considered irrelevant in the following discussion.

The EIS was also recorded to study charge-transfer rates on these catalysts, which also were of importance for the ORR process. Fig. 6 shows the Nyquist plots for these catalysts at the open circuit potential, which displayed similar characteristics corresponding to reflective finite diffusive systems. At very high frequencies, the system behaved like a pure resistance while at low frequencies it was analogous to a pure capacitance. In the middle frequency domain, the influence of the electrode porosity is significant. Thus, an equivalent circuit was employed to represent the impedance behaviours of this kind of system, as shown in the inset of Fig. 6. According to the simulated parameters listed in Table 1, the catalyst film resistances (R_f, containing the solution resistance) were similar for all the catalysts. It seems that the Fe species did not affect the bulk electronic conductivity of the final catalysts. However, the charge-transfer resistance (R_{ct}) of 10Fe–PANI-L was obviously larger than that of other samples, which revealed the slower charge-transfer rates at the interface between of the catalyst and the electrolyte. This could be part of the reason for its lower ORR activity.

The stability of the polyaniline based catalysts has been a critical concern. Wu et al. performed a 700-h fuel-cell performance test at a constant cell voltage of 0.4 V with PANI-based catalysts, showing

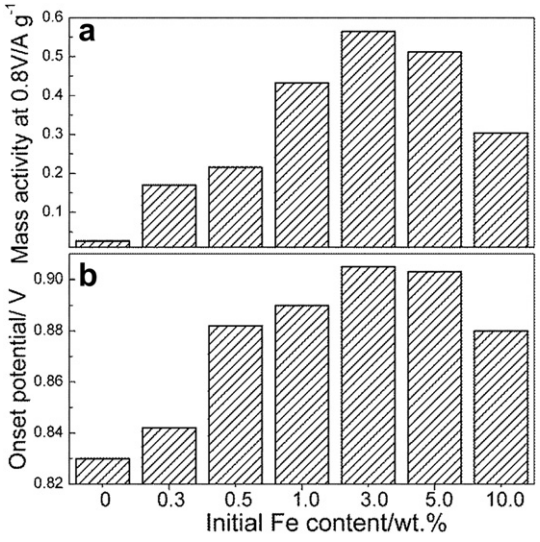

Fig. 4. (a) Kinetic current densities at 0.8 V derived from Tafel graphs and (b) onset ORR potentials for the catalysts depicted in Fig. 2.

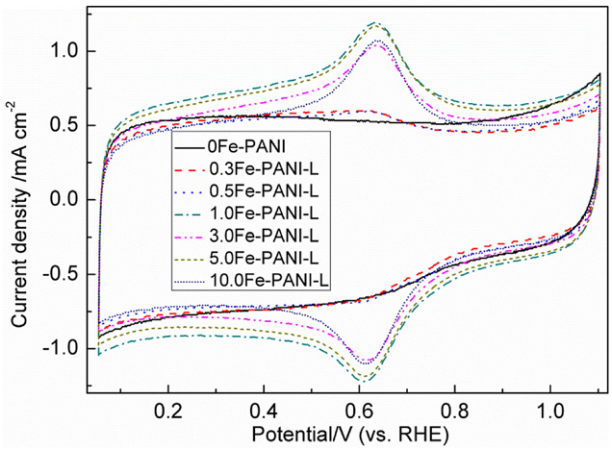

Fig. 5. Cyclic voltammograms of 0Fe–PANI, 0.3Fe–PANI-L, 0.5Fe–PANI-L, 1.0Fe–PANI-L, 3.0Fe–PANI-L, 5.0Fe–PANI-L and 10.0Fe–PANI-L in N_2-saturated pH 1 H_2SO_4 solution with a sweep rate of 10 mV s^{-1}. Catalyst loading: 0.6 mg cm^{-2}.

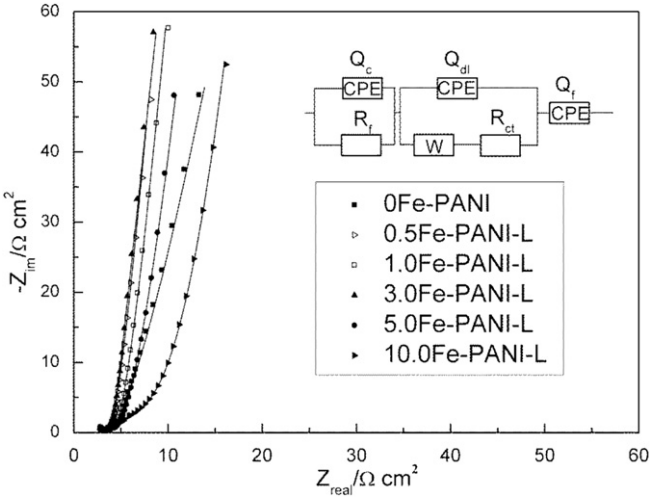

Fig. 6. Nyquist plots of EIS of 0Fe–PANI, 0.5Fe–PANI-L, 1.0Fe–PANI-L, 3.0Fe–PANI-L, 5.0Fe–PANI-L and 10.0Fe–PANI-L recorded in N_2 saturated pH 1 H_2SO_4 solution at the open circuit potential. The inset is the equivalent circuit used for fitting the experimental data: Q_c, constant phase element related to the capacitance at the contact interface between glassy carbon and catalyst film; R_f, catalyst film resistance (incorporating the solution resistance); W, Warburg impedance; R_{ct}, charge transfer resistance; Q_{dl}, constant phase element related to double layer capacitance; Q_f, constant phase element related to carbon film capacitance. The solid lines show the fitted curves.

Table 1
The best fitting values of equivalent circuit elements from Fig. 6

Sample	$Q_c \times 10^7/\Omega^{-1}$ s^{n1} cm^{-2}	n_1	R_f/Ω cm^2	W/Ω cm^{-2} $s^{0.5}$	R_{ct}/Ω cm^2	$Q_{dl} \times 10^2/\Omega^{-1}$ s^{n2} cm^{-2}	n_2	$Q_f \times 10^2/\Omega^{-1}$ s^{n3} cm^{-2}	n_3
0Fe–PANI	4.38	0.911	3.010	0.1475	0.920	0.22	0.916	3.575	0.941
0.5Fe–PANI-L	2.68	0.949	3.024	0.3618	0.727	0.95	0.747	3.500	0.974
1.0Fe–PANI-L	3.09	0.939	3.078	0.2687	1.298	0.86	0.706	2.892	0.974
3.0Fe–PANI-L	1.81	0.997	2.593	0.1896	0.499	1.10	0.721	2.726	0.950
5.0Fe–PANI-L	3.99	0.921	3.162	0.1853	1.453	0.82	0.673	3.622	0.974
10.0Fe–PANI-L	2.59	0.954	3.070	0.0904	6.591	1.50	0.587	3.661	1.0

good durability at the fuel cell cathode [16]. The catalyst stability was also investigated in this work using chronoamperometry (at 0.734 V) in the O_2 bubbled H_2SO_4 electrolyte (data not shown here). After 2 h, about 63% of the initial current remained for the 3.0Fe–PANI-L electrode while 73% for the Pt/C electrode. This preliminary result indicated the promising stability of this kind of catalysts. Evaluation of the long-term stability should be the subject of further study of this type of catalysts, preferably considering the formation of hydrogen peroxide intermediates.

3.3. EBSD and TEM

Considering the notable contrast difference between Fe and C, N and possible detriment of magnetic Fe species to the TEM instrument, EBSD may be a better technique to detect the metallic particles in carbon substrates on a large scale. Fig. 7 shows the EBSD images of 3Fe–PANI, 3Fe–PANI-L and 5Fe–PANI-L. As shown in Fig. 7a, the sparse Fe-containing nanoparticles (white points in the figure) with a diameter of *ca.* 300 nm were deposited on the surface of the 3Fe–PANI catalyst. After the acid leaching treatment, Fig. 7b shows no visible Fe-containing nanoparticles either on a 2 μm or 500 nm scale. For 5Fe–PANI-L, however, some tiny Fe-containing particles could be detected. The representative TEM image for the leached 3Fe–PANI-L is shown in Fig. 7d, where no ordered structure is observed in the leached sample consisting primarily of amorphous carbon. These results indicated that the Fe-containing particles encapsulated in the carbon matrix should not be the origin of the high ORR activity of 3Fe–PANI-L. Besides, the TEM images herein were slightly different from those of previous reports [7], in which many metal-containing particles were detected. It might originate from the different synthesis procedures used.

3.4. XPS analysis

To get a full understanding of the surface composition of the prepared catalysts, XPS measurements were carried out. N 1s and O 1s spectra for selected samples are compared in Fig. 8. Detailed information about the molecular structure scheme of heterocyclic N compounds has been described in previous reports [32,42]. In this work, all spectra of N 1s were fitted well with four peaks that are known to originate from pyridinic (N1, at *ca.* 398.33 eV), pyrrolic (N2, at *ca.* 399.8 eV), quaternary (N3, at *ca.* 401 eV) and oxidized type of (N4, at *ca.* 402.3 eV) nitrogen. The deconvolution results are listed in Table 2. For samples from 0.5Fe–PANI-L to 5Fe–PANI-L, the N surface contents were found to be in a narrow range from *ca.* 3.0 to 3.5 at.%. No clear correlation could be found between the surface nitrogen content and catalytic activities of these catalysts. The total nitrogen content of 3.0 at.% seems to be enough for the formation of the active sites in all the six catalysts, which does not seem to be the limiting factor. For the 3Fe–PANI-L catalyst which exhibited the best ORR activity, the N contents of pyridinic and pyrrolic origin were relatively higher than those of other catalysts.

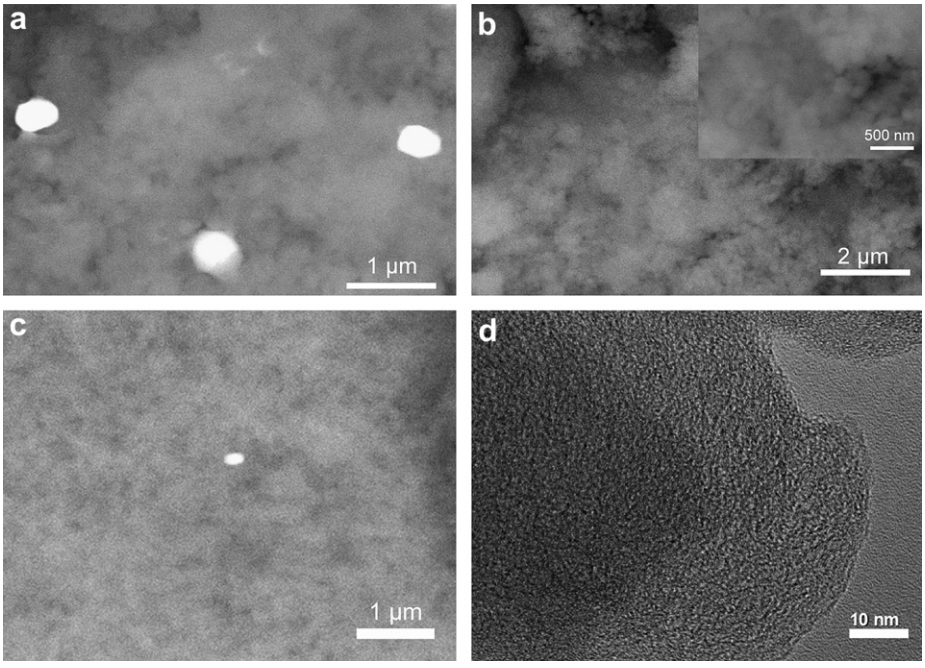

Fig. 7. EBSD images of (a) 3.0Fe-PANI, (b) 3.0Fe–PANI-L, (c) 5.0Fe–PANI-L and HRTEM image of (d) 3.0Fe–PANI-L.

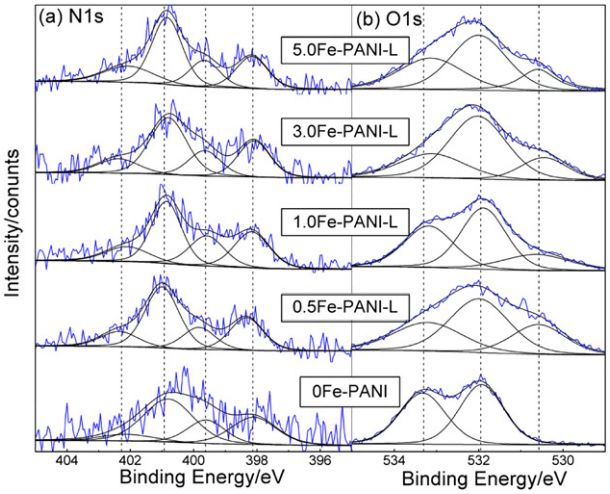

Fig. 8. XPS spectra of (a) N 1s and (b) O 1s core-level for 0Fe–PANI, 0.5Fe–PANI-L, 1.0Fe–PANI-L, 3.0Fe–PANI-L and 5.0Fe–PANI-L.

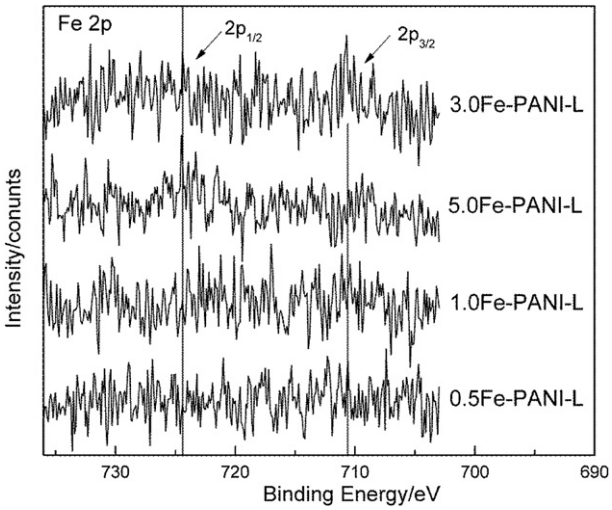

Fig. 9. XPS spectra in the Fe 2p region for 0.5Fe–PANI-L, 1.0Fe–PANI-L, 3.0Fe–PANI-L and 5.0Fe–PANI-L.

The O 1s XPS spectra for the five samples are also presented in Fig. 8. The spectra could be deconvoluted into three components: O1 (at *ca.* 530.6 eV), O2 (at *ca.* 531.9 eV) and O3 (at *ca.* 533.2 eV). The O1 was assigned to the S–O (sulphate species) groups, O2 to the C–OH and/or C–O–C groups and O3 to the C=O groups [43,44]. For the spectrum of the 0Fe–PANI, only O2 and O3 components were identified while all these three components were involved in other samples. In view of the differences in the preparation and other results in literature [44], the O1 component should be brought during the acid leaching process. All fitted deconvolution results are collected in Table 2. It is interesting to note that the content of C=O group for the 0Fe–PANI was superior to that of other samples. This might suggest that the surface of the 0Fe–PANI was susceptible to oxidation without Fe species on the surface. In addition, as depicted in Table 2, the nitrogen surface content of 0Fe–PANI was lower than that of others, indicating a fact that the formation of C=O groups on the catalyst surface might lead to reduction of the nitrogen surface content remarkably. This, however, may not necessarily affect the bulk nitrogen content (Table 2). It seems that oxygen tends to interact with carbon to form C=O groups, which would prevent the doped nitrogen on the surface of catalysts. Further investigations are needed to clarify this issue. Concerning the relation between the near-surface oxygen content and the ORR activity, it should be remarked that oxygen was not assumed to be part of active sites [2,45]. Alternatively, the surface incorporated oxygen might affect the doping of nitrogen into the carbon structure and in turn play a role in the catalytic activity.

With regard to the Fe surface content, only a small amount of Fe was detected on the 3Fe–PANI-L sample (*ca.* 0.1 at.%) while the signals of Fe species were buried in the background for the other samples (Fig. 9). This indicated that the metal on the surface was nearly completely leached out during the acid treatment and that a higher Fe content in the precursor might not necessarily lead to higher Fe surface content on the final catalyst. No efforts were hence made to correlate the actual Fe surface content and the ORR activity in the final catalysts.

3.5. XRD

Fig. 10 shows the XRD patterns of the *X*Fe–PANI ($X = 0, 1, 3, 5, 10$) and *X*Fe–PANI-L ($X = 1, 3, 5, 10$) samples. In these spectra, the strong peak around $2\theta = 26.4^\circ$ and weaker peak around $2\theta = 44.5^\circ$ were assumed to correspond to the (002) and (100) diffractions in the graphitic structure while the broad peaks were attributed to the amorphous and graphitic carbon. The XRD pattern for 10Fe–PANI showed the characteristic diffraction peaks that could be assigned to a mixture of Fe_3C (JCPDS 35–0772), a small amount of Fe_xS (*e.g.*, JCPDS 76–0962) and αFe (JCPDS 06–0696). In cases of *X*Fe–PANI ($X = 1, 3, 5$) catalysts only a small amount of Fe_xS and αFe aggregates were detected. No Fe_xO crystallines were detectable in all samples, for which the possible reason had been discussed before. After being leached, only a small amount of Fe_xS (probably with traces of αFe) was detected in 10Fe–PANI-L, while no crystalline structure of Fe-containing phases were found in other samples. From the EDX spectra of PANI-2 (not shown here), a small amount of sulphur (*ca.* 2.94 at.%) is recognized. Any sulfide compounds might exhibit a higher reactivity than that of hydrocarbons because of their higher electronegativity and consequently they could easily react with $FeCl_3$ or its pyrolytic products to form Fe_xS compounds. The compounds might eventually be transformed into α-Fe when further heat-treated at high temperature [46]. As a result, Fe_xS and αFe were first formed in the *X*Fe–PANI ($X = 1, 3$) samples. When the quantity of the added

Table 2
Surface atomic concentrations of N, O, Fe, different nitrogen and oxygen groups in selected catalysts calculated from XPS results, and N bulk content determined by EDX.

Sample	N content (at.%)	N bulk content (at.%)	N1 (at.%)	N2 (at.%)	N3 (at.%)	N4 (at.%)	O content (at.%)	O1 (%)	O2 (%)	O3 (%)	Fe content (at.%)
0Fe–PANI	1.02	5.3	0.27	0.19	0.47	0.08	12.4	53.9	47.1	NA[b]	BD[c]
0.5Fe–PANI-L	3.49	–[a]	0.76	0.61	1.52	0.60	10.53	25.5	57.6	16.9	BD
1.0Fe–PANI-L	2.95	4.8	0.73	0.52	1.33	0.37	13.13	37.4	50.8	11.8	BD
3.0Fe–PANI-L	3.54	4.8	0.93	0.77	1.37	0.47	10.84	28.0	48.0	24.0	0.1
5.0Fe–PANI-L	3.43	3.9	0.84	0.55	1.60	0.44	11.14	33.2	50.8	16.0	BD

[a] The EDX experiment was not performed for the 0.5Fe–PANI-L.
[b] O3 component was not involved in the fitted spectrum for the 0Fe–PANI.
[c] Fe surface contents were below the detection threshold for these samples.

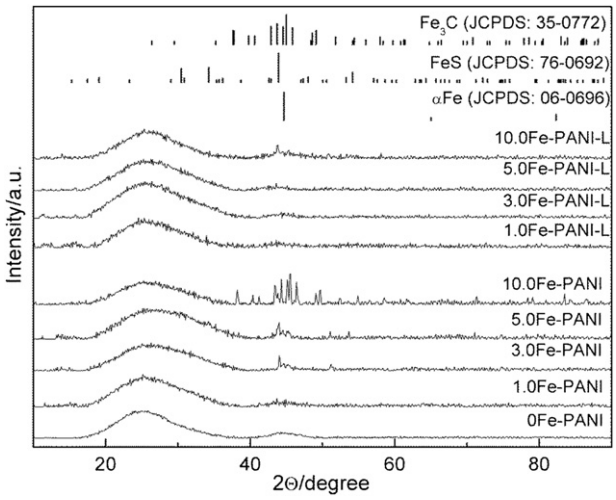

Fig. 10. XRD patterns for 0Fe–PANI, 1.0Fe–PANI, 3.0Fe–PANI, 5.0Fe–PANI, 10.0Fe–PANI and 1.0Fe–PANI-L, 3.0Fe–PANI-L, 5.0Fe–PANI-L, 10.0Fe–PANI-L.

$FeCl_3$ was more than that needed for reaction with sulfide compounds such as 5 and 10 wt.%, Fe_3C could be formed in the co-carbonization products, primarily on the surface of samples as shown in Fig. 10. In the process of the acid leaching, the Fe_3C would first be removed. As a result, a small amount of Fe_xS was detected in 10Fe–PANI-L. Combining the CV results, possible Fe_xO species might be buried in the carbon matrix, which protected them in the leaching process. In view of the low catalytic activity of the 10Fe–PANI-L catalyst, the Fe_xS phase should have little ORR activity but might be responsible to the large R_{ct} observed, as discussed above.

4. Conclusions

Self-supported, nanoworm-shaped non-precious metal catalysts (NPMCs) for the ORR were synthesized with pre-prepared polyaniline nanofibers as both nitrogen and carbon precursors. The nanostructures of the PANI precursor were found to be primarily preserved during the synthesis and the following treatments of NPMCs. This finding opens the possibility of tailoring structures of prepared NPMCs by employing nano-structured precursors. The onset ORR potential of 0.905 V *vs*. RHE and nearly four-electron pathway of prepared catalysts were found, evidencing the formation of active sites with high intrinsic catalytic activity. The onset ORR potential and ORR activity were significantly improved as the initial Fe content in the precursor was increased from 0 to 3.0 wt.%. Further increase of the Fe content in the precursor led to a decrease in the catalytic activity, probably originating from the non-active phase (*eg.* Fe_xS and Fe_xO) remained after the acid leach process.

Acknowledgements

This work was supported by National Natural Science Foundation of China (21011130027, 20933004), National Basic Research Program of China (973 Program, 2012CB215500, 2012CB932800), Danish National Research Foundation and Danish ForskEL programme.

References

[1] B.C.H. Steele, A. Heinzel, Nature 414 (2001) 345–352.
[2] M. Lefevre, E. Proietti, F. Jaouen, J.P. Dodelet, Science 324 (2009) 71–74.
[3] B.M. Fabuss, A. Korosi, D.F. Othmer, Journal of Chemical & Engineering Data 14 (1969) 192–197.
[4] F. Jaouen, E. Proietti, M. Lefevre, R. Chenitz, J.P. Dodelet, G. Wu, H.T. Chung, C.M. Johnston, P. Zelenay, Energy & Environmental Science 4 (2011) 114–130.
[5] L. Zhang, J.J. Zhang, D.P. Wilkinson, H.J. Wang, Journal of Power Sources 156 (2006) 171–182.
[6] R. Bashyam, P. Zelenay, Nature 443 (2006) 63–66.
[7] G. Wu, C.M. Johnston, N.H. Mack, K. Artyushkova, M. Ferrandon, M. Nelson, J.S. Lezama-Pacheco, S.D. Conradson, K.L. More, D.J. Myers, P. Zelenay, Journal of Materials Chemistry 21 (2011) 11392–11405.
[8] H.M. Zhang, X.H. Wang, J. Li, Z.S. Mo, F.S. Wang, Polymer 50 (2009) 2674–2679.
[9] M.S. Thorum, J. Yadav, A.A. Gewirth, Angewandte Chemie 121 (2009) 171–173.
[10] R. Jasinski, Nature 201 (1964) 1212.
[11] S. Gupta, D. Tryk, I. Bae, W. Aldred, E. Yeager, Journal of Applied Electrochemistry 19 (1989) 19–27.
[12] K.L. Hsueh, D.T. Chin, S. Srinivasan, Journal of Electroanalytical Chemistry and Interfacial Electrochemistry 153 (1983) 79–95.
[13] G. Wu, Z. Chen, K. Artyushkova, F.H. Garzon, P. Zelenay, ECS Transactions 16 (2008) 159–170.
[14] H.S. Liu, Z. Shi, J.L. Zhang, L. Zhang, J.J. Zhang, Journal of Materials Chemistry 19 (2009) 468–470.
[15] G. Wu, M.A. Nelson, N.H. Mack, S.G. Ma, P. Sekhar, F.H. Garzon, P. Zelenay, Chemical Communications 46 (2010) 7489–7491.
[16] G. Wu, K.L. More, C.M. Johnston, P. Zelenay, Science 332 (2011) 443–447.
[17] H. Meng, N. Larouche, M. Lefevre, F. Jaouen, B. Stansfield, J.P. Dodelet, Electrochimica Acta 55 (2010) 6450–6461.
[18] H.R. Byon, J. Suntivich, E.J. Crumlin, Y. Shao-Horn, Physical Chemistry Chemical Physics 13 (2011) 21437–21445.
[19] G. Liu, X. Li, P. Ganesan, B.N. Popov, Applied Catalysis B: Environmental 93 (2009) 156–165.
[20] G. Liu, X. Li, P. Ganesan, B.N. Popov, Electrochimica Acta 55 (2010) 2853–2858.
[21] F. Jaouen, S. Marcotte, J.P. Dodelet, G. Lindbergh, Journal of Physical Chemistry B 107 (2003) 1376–1386.
[22] F. Jaouen, J.P. Dodelet, Journal of Physical Chemistry C 113 (2009) 15422–15432.
[23] Y. Zhu, J.M. Li, M.X. Wan, L. Jiang, European Journal of Inorganic Chemistry (2009) 2860–2864.
[24] D.-s. Yuan, T.-x. Zhou, S.-l. Zhou, W.-j. Zou, S.-s. Mo, N.-n. Xia, Electrochemistry Communications 13 (2011) 242–246.
[25] M. Kyotani, H. Goto, K. Suda, T. Nagai, Y. Matsui, K. Akagi, Journal of Nanoscience and Nanotechnology 8 (2008) 1999–2004.
[26] P. Bogdanoff, I. Herrmann, G. Schmithals, S. Fiechter, ECS Transactions 3 (2006) 211–219.
[27] I. Galbiati, C.L. Bianchi, M. Longhi, A. Carra, L. Formaro, Fuel Cells 10 (2010) 251–258.
[28] F. Jaouen, J.P. Dodelet, Electrochimica Acta 52 (2007) 5975–5984.
[29] P.H. Matter, E. Wang, M. Arias, E.J. Biddinger, U.S. Ozkan, Journal of Physical Chemistry B 110 (2006) 18374–18384.
[30] V. Nallathambi, J.W. Lee, S.P. Kumaraguru, G. Wu, B.N. Popov, Journal of Power Sources 183 (2008) 34–42.
[31] A. Rahy, M. Sakrout, S. Manohar, S.J. Cho, J. Ferraris, D.J. Yang, Chemistry of Materials 20 (2008) 4808–4814.
[32] F. Jaouen, J. Herranz, M. Lefevre, J.P. Dodelet, U.I. Kramm, I. Herrmann, P. Bogdanoff, J. Maruyama, T. Nagaoka, A. Garsuch, J.R. Dahn, T. Olson, S. Pylypenko, P. Atanassov, E.A. Ustinov, ACS Applied Materials and Interfaces 1 (2009) 1623–1639.
[33] M. Trchová, E.N. Konyushenko, J. Stejskal, J. Kovárová, G. Ćirić-Marjanović, Polymer Degradation and Stability 94 (2009) 929–938.
[34] H. Gershi, A. Geclanken, H. Keppner, H. Cohen, Carbon 49 (2011) 1067–1074.
[35] P.P. George, V.G. Pol, Y. Koltypin, M.S. Ben-David, I. Genish, A. Gedanken, Rsc Advances 1 (2011) 619–624.
[36] A. Wroblewska, A. Fajdek, Journal of Advanced Oxidation Technologies 14 (2011) 122–130.
[37] Z. Liu, Y. Liu, S. Poyraz, X. Zhang, Chemical Communications 47 (2011) 4421–4423.
[38] J.-H. Zhao, H.-L. Li, Q. Lin, K.-X. Li, Z. Peng, X.-S. Zhao, Chemical Journal of Chinese Universities-Chinese 31 (2010) 1088–1092.
[39] G. Wu, D.Y. Li, C.S. Dai, D.L. Wang, N. Li, Langmuir 24 (2008) 3566–3575.
[40] S.J. Liu, C.H. Huang, C.K. Huang, W.S. Hwang, Chemical Communications (2009) 4809–4811.
[41] B. Ha, O.H. Han, K.J. Hwang, S. Kim, C.K. Rhee, Electrochimica Acta 58 (2011) 422–426.
[42] P.H. Matter, L. Zhang, U.S. Ozkan, Journal of Catalysis 239 (2006) 83–96.
[43] C. Kozlowski, P.M.A. Sherwood, Journal of the Chemical Society, Faraday Transactions 1: Physical Chemistry in Condensed Phases 81 (1985) 2745–2756.
[44] G.X. Zhang, S.H. Sun, D.Q. Yang, J.P. Dodelet, E. Sacher, Carbon 46 (2008) 196–205.
[45] M. Lefèvre, J.P. Dodelet, P. Bertrand, The Journal of Physical Chemistry B 106 (2002) 8705–8713.
[46] U.I. Kramm, I. Herrmann, S. Fiechter, G. Zehl, I. Zizak, I. Abs-Wurmbach, J. Radnik, I. Dorbandt, P. Bogdanoff, ECS Transactions 25 (2009) 659–670.